Effects of Subscale Size and Shape on Global Energy Dissipation in a Multiscale Model of a Fiber-reinforced Composite Exhibiting Post-peak Strain Softening using Abaqus and FEAMAC

Evan J. Pineda, Brett A. Bednarcyk, and Steven M. Arnold

NASA Glenn Research Center, 21000 Brookpark Rd., Cleveland, OH 44135

Abstract: A mesh objective crack band model is implemented in the generalized method of cells (GMC) micromechanics model to predict failure of a composite repeating unit cell (RUC). The micromechanics calculations are achieved using the MAC/GMC core engine within the ImMAC suite of micromechanics codes, developed at the NASA Glenn Research Center. The microscale RUC is linked to a macroscale Abaqus/Standard finite element model using the FEAMAC multiscale framework (included in the ImMAC suite). The effects of the relationship between the characteristic length of the finite element and the size of the microscale RUC on the total energy dissipation of the multiscale model are investigated. A simple 2-D composite square subjected to uniaxial tension is used to demonstrate the effects of scaling the dimensions of the RUC such that the length of the sides of the RUC are equal to the characteristic length of the finite element. These results are compared to simulations where the size of the RUC is fixed, independent of the element size. Simulations are carried out for a variety of mesh densities and element shapes, including square and triangular. Results indicate that a consistent size and shape must be used to yield preserve energy dissipation across the scales.

Keywords: Composites, Continuum Damage Mechanics, Constitutive Modeling, Multiscale Modeling, Progressive Damage, Progressive Failure, FEAMAC, MAC/GMC, ImMAC, Abaqus/Standard, Crack Band, Smeared Crack, Mesh Objective Failure, Length Scaling.

1. Introduction

Often, details at the constituent level drive the failure of a composite material. An effective way to incorporate these details into a numerical model is through multiscale analysis. However, careful attention must be paid to how failure is modeled at the different scales. If the stress-strain response of the material enters the post-peak softening regime and the tangent stiffness tensor looses positive definiteness, the results become sensitive to changes in the mesh. Even if mesh objective constitutive models are in place at the microscales or macroscales, mesh objectivity is not necessarily maintained across the scales, and the resulting multiscale model will still exhibit pathological dependence on the size of the discretizations in one or more scales due to the lack of a clearly defined characteristic length(s) that bridges the scales (Bažant, 2007).

A multiscale model is presented here which couples the generalized method of cells (GMC) micromechanics model (Paley and Aboudi, 1992), to a macroscopic finite element method (FEM) model. The commercial FEM software Abaqus is used as the macroscale platform (Simulia Corp., 2008). Whereas, the openly distributed Integrated Multiscale Micromechanics Analysis Code

(ImMAC) suite of micromechanics codes, developed by the NASA Glenn Research Center (GRC), is utilized to perform the microscale calculations (Bednarcyk and Arnold, 2002a; Bednarcyk and Arnold, 2002b). The Micromechanics Analysis Code/Generalized Method of Cells (MAC/GMC) core engine, within the ImMAC suite, is used to implement and solve the subscale GMC problem, and the FEAMAC multiscale framework (Bednarcyk and Arnold, 2006) facilitates the communication between Abaqus and MAC/GMC via Abaqus user subroutines.

A mesh objective crack band model (Bažant and Oh, 1983) was implemented at the subcell level within the GMC micromechanics model. With the crack band model, the negative, post peak, tangent slope of the stress-strain response of the material is scaled so that the strain energy release rate (SERR) of the subcell equals the critical fracture toughness of the material when the stress in the subcell has diminished to zero. The crack band model at the microscale is used to influence the behavior of the macroscale, in the multiscale FEAMAC model. Pineda et al. (2012) previously implemented the crack band model within the high fidelity generalized method of cells (HFGMC), and demonstrated the objectivity of the HFGMC solution with respect to the subcell meshes used in the repeating unit cell (RUC). By extension, it is assumed that mesh objectivity is assured within the GMC framework at the microscale, but this does not warrant mesh objectivity at the macroscale.

The objective of this work is to investigate the effect of the size and shape of the subscale RUC, related to the macroscale finite element, on the preservation of energy in the multiscale model. Thus, a simple example problem is presented to demonstrate these effects. A square, two-dimensional (2-D), plane strain composite section was loaded in uniaxial tension, and failure was allowed to evolve within microscale RUCs that were linked to the macroscale with FEAMAC. The overall SERR of the model was calculated when the dimensions of the RUC were scaled such that the length of the sides of the RUC are equal to the characteristic length of the macroscale finite element, and the SERR of the multiscale model was also calculated when the dimensions of the RUC were fixed to a realistic value. The calculations were performed for numerous macroscale FEM mesh densities and shapes (including square and triangular).

2.   Modeling Progressive Failure at the Microscale

A micromechanical analysis technique, coined the method of cells (MOC), was developed by Aboudi (1991); subsequently, Paley and Aboudi (1992) expanded MOC into the generalized method of cells (GMC), and later Aboudi et al. (2001) further increased the robustness of this method with the high fidelity generalized method of cells (HFGMC). These methods provide semi-closed form solutions for determining global anisotropic composite properties in terms of the constituent materials, as well as the full three dimensional (3-D) stresses and strains in each of the constituent subcells.

2.1   The Generalized Method of Cells

It is assumed that a continuously reinforced composite microstructure can be represented as a collection of doubly-periodic RUCs containing a general number of constituents, as shown in Figure 1. The RUC is then discretized into N_β x N_γ rectangular subcells, as exhibited in Figure 2. Each of these subcells is occupied by one of the constituent materials of the composite. The number of subcells and the number of materials are completely general.

Displacement and traction continuity are enforced in an average, integral sense at the subcell interfaces of a discretized RUC. These continuity conditions are used to formulate a set of semi-analytical linear algebraic equations that are solved for the local subcell strains in terms of globally applied strains or stresses. Subsequently, local constitutive laws can be utilized to obtain the local subcell stresses, and a constitutive law for the effective, homogenized composite can be formulated. GMC and HFGMC were later reformulated reducing the total number of unknowns required to define the problem by Pindera and Bednarcyk (1997) and Aboudi et al. (2012), respectively.
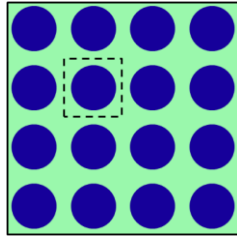
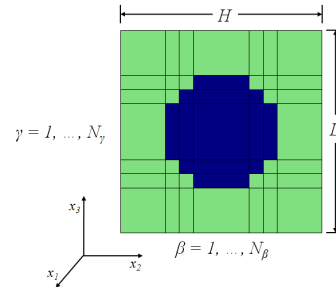**Figure 1. Representation of the doubly-periodic microstructure of a composite material.**

Figure 2. Discretization of a doubly-periodic RUC.

2.2   Implementation of a Smeared Crack Band Model

When materials enter the post-peak strain softening regime (i.e. failure), stress is related to strain through a negative tangent stiffness. If the tangent stiffness tensor looses positive definiteness, failure localizes to the smallest length scale in the continuum problem (Bažant and Cedolin, 1991). In FEM this is a single element, and in GMC this is a single subcell. Thus, the post-peak strain softening energy is dissipated over the volume of the discretization entity it localizes to. Since a stress-strain relationship prescribes the energy density dissipated during the failure process, the total amount of energy dissipated in the local volume decreases if the size of that local volume is reduced, and in the limit the structure would theoretically require zero energy to fail. This pathological mesh dependence of numerical simulations utilizing constitutive laws containing a negative tangent stiffness that relates stresses to strains is well documented in the literature (Bažant and Cedolin, 1979; Pietruszczak and Mroz, 1981; deBorst, 1987).

One way to overcome this mesh dependence is the use of non-local constitutive laws, which utilize the strain gradients to introduce the influence of surrounding elements into the stress-strain behavior of a failing element, preventing localization (Eringen, 1996; Bažant, 1994). A more tractable method involves judiciously scaling the post-peak softening slope of the stress-strain curve. Then, the energy density dissipated via failure is a function of the characteristic length within the discretized continuum, and the strain energy release rate (SERR) (energy required to create a unit area of new crack surface) is preserved despite changes in the size of the mesh. This type of constitutive law is referred to as a crack band, or smeared crack, model (Bažant and Oh, 1983; de Borst and Nauta, 1985).

A variation of the crack band model was implemented in HFGMC by Pineda et al. (2012), and was also implemented in GMC for this work. Crack band initiation is determined using a maximum principal stress criterion.

$$\frac{\overline{\sigma}_1^{(\beta\gamma)}}{\sigma_C^{(\beta\gamma)}} = 1, \qquad \overline{\sigma}_1^{(\beta\gamma)} \geq 1 \tag{1},$$

where $\overline{\sigma}_1^{(\beta\gamma)}$ is the maximum principal stress, and $\sigma_C^{(\beta\gamma)}$ is the mode I cohesive strength of the material. Upon initiation, the crack band is oriented such that the normal to the crack band $n_1^{(\beta\gamma)}$ is aligned with the direction of maximum principle stress. Figure 3 displays a crack band within a discretized continuum, and a magnified view of a single subcell shows the crack band of width w_C oriented perpendicular to $n_1^{(\beta\gamma)}$. The characteristic length of the subcell $l_C^{(\beta\gamma)}$ is taken as the length of a line running across the subcell, oriented in the direction of $n_1^{(\beta\gamma)}$.
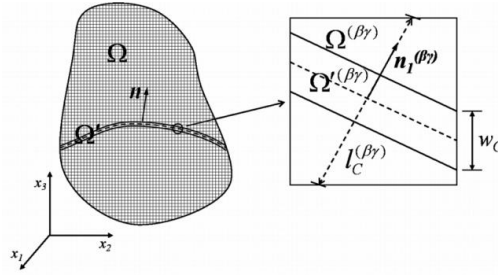

Figure 3. (Left) Crack band embedded in a discretized continuum. (Right) Magnified subcell displays crack band orientation within subcell, as well as characteristic length of subcell.
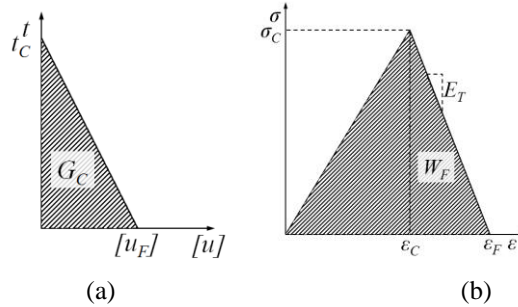

(a)   (b)

Figure 4. (a) Traction separation law governing behavior of crack band. (b). Stress-strain behavior of material.

The behavior of the crack band is controlled by a traction t versus separation $[u]$ law, shown in Figure 4a. The traction-separation law prescribes that the SERR of the subcell (given by the area under the traction separation curve) is equal to the fracture toughness, or critical SERR (G_C), of the material when the traction reaches zero. Since no actual discontinuity is present within the GMC subcell, the subcell behaves as a continuum and obeys a stress versus strain constitutive law, displayed in Figure 4b. The dissipated strain energy density W_F is the area under the stress-strain

2012 SIMULIA Customer Conference

curve. Additionally, the stress state in a subcell is uniform; therefore, the subcell stresses and tractions on the crack band are equivalent. To ensure mesh objectivity, the negative, post-peak softening slope of the stress-strain curve E_T is adjusted so that, for subcell $\beta\gamma$ which contains the crack band,

$$l_C^{(\beta\gamma)}W_F^{(\beta\gamma)}\left(l_C^{(\beta\gamma)}\right) = G_{IC}^{(\beta\gamma)} \tag{2},$$

where $l_C^{(\beta\gamma)}$ is the characteristic length of the subcell, defined in Figure 3, $W_F^{(\beta\gamma)}$ is the total strain energy density, which is dependent on $l_C^{(\beta\gamma)}$, that is dissipated in the subcell when the stress reaches zero, and $G_{IC}^{(\beta\gamma)}$ is the fracture toughness of the material occupying the subcell (material property). Equation (2 ensures objectivity with respect to changes in the subcell mesh by maintaining that the total SERR, upon complete failure (i.e. completely diminished stress), in the subcell is fixed and independent of the size of the subcell. For complete details on the implementation of the crack band model, please refer to Pineda et al. (2012).

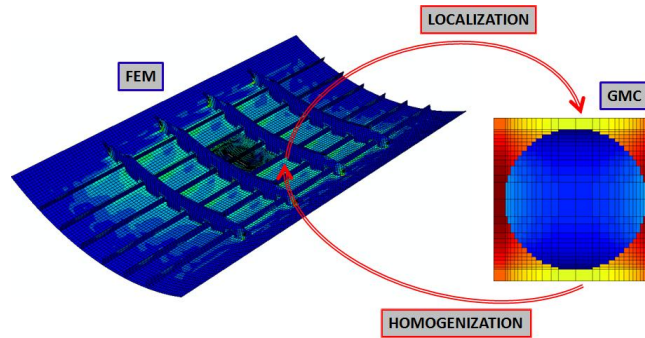## 3. FEAMAC Multiscale Framework

Figure 5. Diagram showing coupling of macroscale FEM and microscale GMC models.

A multiscale framework is utilized to simulate the deformational response of fiber-reinforced composite structures by modeling the fiber-matrix architecture as an RUC at the microscale using GMC and coupling the microscale to the lamina/laminate level (macrsocale) FEM model. A synergistic approach is employed which executes concurrent multiscaling in time, but sequential in length (Sullivan and Arnold, 2011). The commercial finite element software, Abaqus 6.10-1 (Simulia Corp., 2008), is used as the FEM platform, and the MAC/GMC core micromechanics software (Bednarcyk and Arnold, 2002a; Bednarcyk and Arnold, 2002b) is used to perform microscale calculations. The scales are linked using the FEAMAC software implementation (Bednarcyk and Arnold, 2006), which utilizes various Abaqus/Standard user subroutines. Subsequently, a wrapper was developed (FEAMAC/Explicit) which achieves the same multiscaling tasks as FEAMAC, except Abaqus/Explicit is used as the FEM platform (Pineda et al., 2009). MAC/GMC, FEAMAC, and FEAMAC/Explicit are available in the openly distributed ImMAC suite of micromechanics codes, developed by NASA GRC. The number of subcells and

constituents within an RUC at the microscale is completely general, and as many, or as few, as needed may be used to accurately characterize the micro-architecture of the composite. Moreover, any constitutive model can be used in the subcells of the RUC to rerpresent the mechanical or thermal response of the constituents.

A schematic displaying a typical multiscale model using FEAMAC is displayed in Figure 5. The integration point strains are applied to the RUC and the local subcell fields are determined using GMC (this process is referred to as localizaion). If the subcell material behavior is nonlinear, the local stresses and strains are used to calculate the local stiffnesses, plastic strains, thermal strains, and/or state variables via the local constitutive law. The RUC is then homogenized and the global stiffnesses, plastic strains, thermal strains, and/or state variables are computed. The global stresses at the integration point are then calculated using these global, homogenized fields, and the effects of any nonlinear subscale phenomena are introduced into the macroscale through changes in the integration point stress state. The global stresses, material jacobian, and updated state variables are then supplied to the Abaqus user material `UMAT` subroutine. For complete details on the FEAMAC implementation, the reader is referred to Bednarcyk and Arnold (2006).

4.   Effect of Subscale Size on Global Energy Dissipation

A mesh objective continuum damage mechanics (CDM) model for post-peak strain softening implemented within the GMC micromechanics framework was presented in Section 2.2. Using such a model ensures that the solutions obtained are insensitive to changes in the subcell mesh (Pineda et al., 2012). Nonetheless, this does not guarantee mesh objectivity if this model is linked to a macroscale model via a multiscale framework. To ensure mesh objectivity the SERR of all elements must be preserved upon changes in the macroscale mesh.

Typically, an RUC is considered dimensionless as the periodic boundary conditions are meant to simulate an infinite array of the RUC. However, the domain of the integration point that the microscale model is coupled to has some finite dimensions. As energy is dissipated at the microscale within the RUC, the macroscale also exhibits energy dissipation governed by the stress-strain response of the homogenized RUC, and this energy is dissipated over the volume of the integration point domain.

The dissipated energy density at the microscale W_D^{RUC} can be calculated as the total energy density minus the elastic strain energy density.

$$W_D^{RUC} = \frac{1}{V^{RUC}} \int \left(\int \sigma_{ij}^{RUC} d\varepsilon_{ij}^{RUC} - \frac{1}{2} \sigma_{ij}^{RUC} \varepsilon_{ij}^{RUC} \right) dV^{RUC} \qquad (3),$$

where ε_{ij}^{RUC} and σ_{ij}^{RUC} are the global, homogenized RUC strain and stress tensor, respectively, and V^{RUC} is the volume of the RUC. Thus, the SERR G^{RUC} can be calculated as the total dissipated energy density multiplied by the characteristic length of the RUC.

$$G^{RUC} = l_C^{RUC} W_D^{RUC} \qquad (4)$$

If the volume of the RUC remains constant for all simulations, then the SERR also remains constant.

Noting that, in a multiscale model, the integration point stress and strains are equivalent to the global stresses and strains of the homogenized RUC, then the dissipated strain energy density is automatically preserved across the scales.

$$W_D^{I.P.} = W_D^{RUC} \tag{5},$$

where $W_D^{I.P.}$ is the dissipated energy density of the integration point. The SERR of the integration point domain $G^{I.P.}$ can be calculated by multiplying Equation (3) by the characteristic length of the integration point domain $l_C^{I.P.}$.

$$G^{I.P.} = l_C^{I.P.} W_D^{RUC} \tag{6}$$

In multiscale simulations that keep the volume of the RUC fixed, the dissipated strain energy density of the RUC W_D^{RUC} is constant, and thus, the SERR is directly proportional to the characteristic length of the integration point domain to which the failure localizes. Consequently as the mesh is refined, the SERR in the localized domains, and thus the entire structure, changes. The results will never converge and are pathologically mesh dependent.

To enact mesh objectivity in the multiscale model, the RUC must preserve the characteristic length of the integration point domain.

$$l_C^{RUC} = l_C^{I.P.} \tag{7}$$

If the characteristic length is preserved, then Equation (**6** becomes

$$G^{I.P.} = G^{RUC} \tag{8},$$

and the SERR of the RUC is preserved within the integration point domain after homogenization. Since the local SERR release rate in the failing subcells is governed by the critical fracture toughness (a fixed material property), the global SERR of the RUC is independent of size. By extension, the SERR of the integration point domain is also insensitive to changes in size.

The challenge in achieving mesh objective multiscale analyses lies in correctly defining the global characteristic length l_C^{RUC}, or $l_C^{I.P.}$. Locally within the RUC, the characteristic length can be defined for a subcell by the orientation of the crack band in the subcell (see Section 2.2). Conversely, in the homogenized RUC, there is no single crack band angle to define the characteristic length. This can be assuaged by defining the RUC such that the dimensions are exactly the same as the dimensions of the integration point domain. Thus, every length that can be defined in the integration point domain is defined equivalently in the RUC, and the characteristic length is automatically preserved across the scales, even if it is unknown.

Unfortunately, in the doubly-periodic GMC micromechanics framework, the shapes of the RUCs are restricted to rectangles; however, 2-D finite elements may take the shape of any general

quadrilateral. The following sections investigate the effects of scaling the size of the RUC to correspond to the volume of the FEM integration point domain on the total SERR of the multiscale model. To demonstrate mesh objectivity, the total SERR of the entire model must be preserved as the FEM mesh is changed.
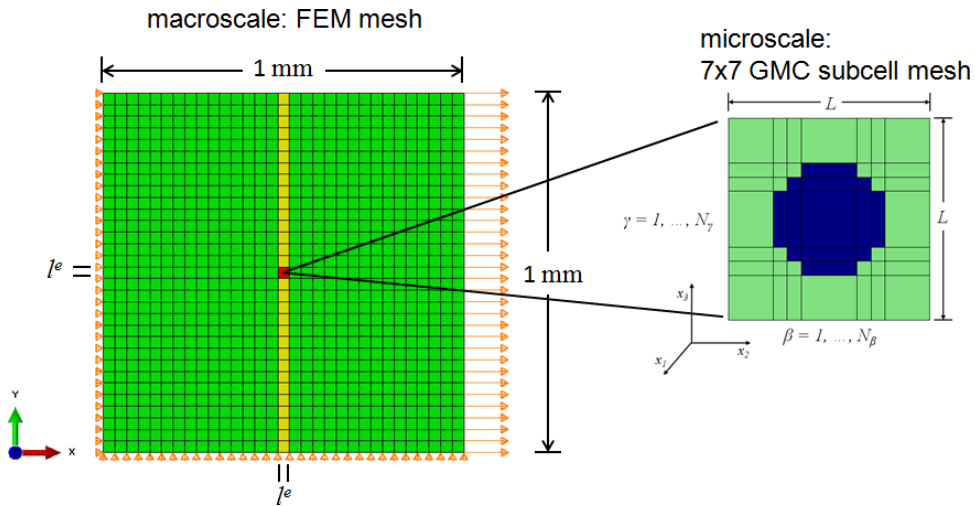
4.1 Numerical Model

Figure 6. Multiscale simulation utilizing square elements at the macroscale

A simple example problem is used to demonstrate the effects of scaling the dimensions of the microscale RUC appropriately on the overall SERR of the multiscale model. Additionally, the effects of using incompatible finite elements and RUC shapes are investigated with the same example problem. Figure 6 exhibits the multiscale example problem. At the macroscale a 1 mm x 1mm square section is modeled using a uniform mesh consisting of square, 2-D, plane strain, reduced integration, CPE4R elements with dimensions l_e x l_e. A global x-y-z coordinate system is employed at the macroscale. The microscale domain is modeled using a doubly-periodic, 7 subcells x 7 subcells GMC RUC with overall dimensions L x L. To maintain the proper aspect ratio, for all RUC sizes, to represent a circular fiber the height and length of the RUC must be equal. The RUC consists of 13 fiber subcells (colored blue) and 36 matrix subcells (colored green), and is meant to represent a square packing architecture. A local x_1-x_2-x_3 coordinate system is used where x_1 is the axial, fiber direction, and x_2/x_3 are the transverse directions. The x_1/z-directions are coincident, as are the x_2/x-directions, and the x_3/y-directions.

The elastic properties of the fiber and matrix constituent subcells were chosen so that the overall elastic response of the homogenized RUC represented the elastic behavior of an IM7/8552 lamina. The transversely elastic properties of IM7/8552 are presented in Table 1 (Camanho et al., 2007), where the x-y plane in Figure 6 is the plane of isotropy and E_{zz} is the axial (fiber direction) Young's modulus, E_{xx} is the transverse stiffness, v_{zx} is the axial Poisson's ratio, and G_{zx} is the axial shear modulus. The matrix subcells in the GMC RUC initially behave as an elastic, isotropic material, and the fibers subcells are initially elastic and transversely isotropic. The initial, elastic properties of the microscale constituents are given in Table 2, where E^m is the matrix Young's

modulus, v^m is the matrix Poisson's ratio, E_{11}^f is the axial fiber Young's modulus in the x_1-direction (see Figure 6), E_{22}^f is the transverse stiffness of the fiber, v_{12}^f and v_{23}^f are the axial and transverse Poisson's ratios, and G_{12}^f is the axial shear stiffness. A fiber volume fraction V^f of 59.1% was used (Camanho et al., 2003). The transverse and axial shear moduli of the fiber were obtained from Goldberg and Gilat (2003). The elastic properties of the matrix and remaining unknown elastic properties of the fiber were calibrated such that the elastic stiffness of the homogenized RUC correlated to the elastic properties of the IM7/8552 lamina.

Table 1. Elastic properties of IM7/8552 lamina (Camanho et al., 2007).

Property		Property	
E_{zz}	171.4 GPa	v_{zx}	0.32
E_{xx}	9.08 GPa	G_{zx}	5.29 GPa

The bottom edge of the FEM domain was pinned in the *y*-direction, and the left edge was pinned in the *x*-direction. A uniform displacement was applied to the right edge of the FEM model to simulate transverse loading of a 1mm x 1mm composite section that stretches infinitely in the global, axial z-direction (plane strain conditions). Due to the high degree of nonlinearity associated with failure, the implicit, dynamic FEM solver available in Abaqus/Standard was utilized to solve the macroscale FEM problem using the keyword `*DYNAMIC`, with the option `APPLICATION = QUASI-STATIC` (Simulia Corp., 2008). A nominal density of 1.57 kg/m^3 was used in all the finite elements. The total displacement (ranging from 0.0175 mm to 0.05 mm), was applied over a time of 1000 seconds.

Table 2. Elastic properties of IM7 carbon fiber and 8552 epoxy matrix constituents used in microscale GMC RUC.

8552 Matrix Properties		IM7 Fiber Properties			
E^m	4.97 GPa	E_{11}^f	286.5 GPa	v_{12}^f	0.29
v^m	0.36	E_{22}^f	12.4 GPa	v_{23}^f	0.29
				G_{12}^f	20.0 GPa

Failure is introduced into the matrix subcells of the microscale RUC, and the effects are transferred to the macroscale through an overall reduction of the stiffness of the RUC (due to a local reduction in the stiffness of the failing matrix subcells). The crack band model presented in Section 2.2 is used to govern failure at the microscale. Only the yellow and red elements in Figure 6 were modeled with multiscale FEAMAC elements. The green elements were modeled using the Abaqus elastic material model and the properties listed in Table 1. Free edge effects and the accuracy of the local fields surrounding the failure path front are influenced by the mesh refinement, to some degree, which may affect the failure path in the simulation. Therefore, failure

was restricted to the yellow and red elements to simplify the problem as much as possible and try to ensure that the energy dissipated in the model is a result of the multiscale methodology, not other influences. Moreover, the matrix subcells of the RUC located in the red element were given a slightly lower cohesive strength than the matrix of the RUCs within the yellow elements. This was imposed to imitate an imperfection and facilitate the localization of initial failure into a single element. Without this imperfection, all of the FEAMAC elements would fail simultaneously because the stress and strain fields are uniform throughout the FEM mesh. After failure initiates in the RUC located in the red element, failure progresses into the RUCs located within the adjacent yellow elements until the failure reaches the free edge of the FEM mesh.

The local mode I cohesive strength $\sigma_C^{(\beta\gamma)}$, and the mode I fracture toughness $G_{IC}^{(\beta\gamma)}$ of the matrix subcells were calibrated using a macroscale mesh of 31 elements x 31 elements. The dimensions of the microscale RUC were chosen to equal the dimension of the finite element; i.e., $L = l^e = 0.0323$ mm. The local parameters were calibrated so that the global ultimate stress and total SERR were close to 60.3 MPa and 0.2774 kJ/m^2, respectively, which are the transverse strength and mode I, transverse fracture toughness for IM7/8552 reported by Camanho et al. (2007). The mode I cohesive strength, and mode I fracture toughness of the matrix that were used in the simulations are displayed in Table 3. It should be noted, that the critical strain of the matrix subcells of the RUCs located in the yellow elements were given a value that was 5% higher than that used in the red element.

Table 3. Crack band failure parameters used in 8552 matrix subcells.

Mode I cohesive strength $\sigma_C^{(\beta\gamma)}$ (Weak)	Mode I fracture toughness $G_{IC}^{(\beta\gamma)}$
56.7 MPa (54.0 MPa)	1.594 kJ/m^2

Simulations were executed using various square meshes, and the total, macroscopic SERR was calculated upon complete diminishment of the load carrying capability. Two scenarios were investigated. The first involved scaling the dimensions of the microscale RUC, so that

$$L = l_C^{I.P.} \tag{9},$$

while retaining $V^f = 59.1\%$. Since reduced integration elements are used, the characteristic length of an element l_C^e, and of the integration point domain in an element $l_C^{I.P.}$, are equivalent.

$$l_C^{I.P.} = l_C^e \tag{10}$$

The characteristic length of a 2-D element is calculated as the square root of the area of the element A^e (Simulia Corp., 2008).

$$l_C^e = \sqrt{A^e} \tag{11}$$

Thus, for a square, reduced integration element, the characteristic length of the integration point domain within an element is equal to the length of one of the sides of the element.

$$l_C^{I.P.} = l^e \tag{12}$$

In the second scenario, the dimension of the RUC was kept fixed at $L = 5.98$ μm (this was calculated assuming a fiber diameter of 5 μm, and retaining a 59.1% fiber volume fraction), while the FEM mesh was refined.
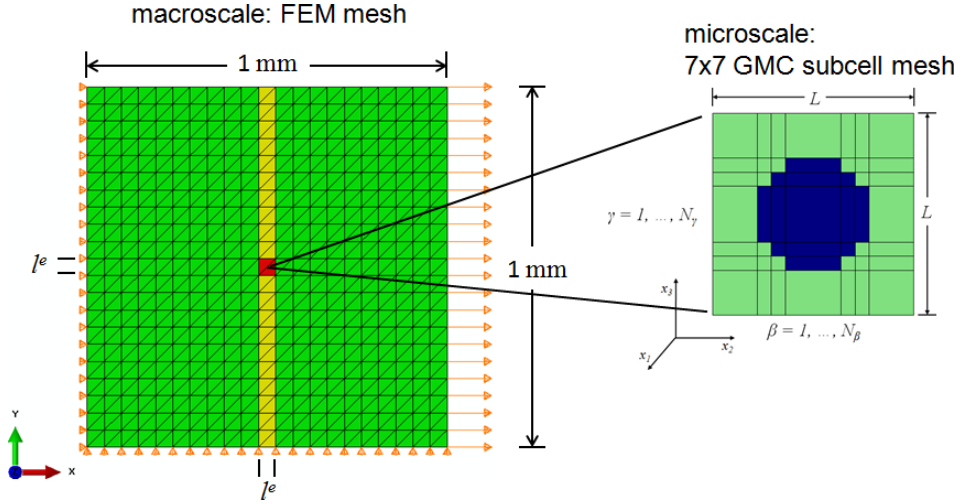

Figure 7. Multiscale simulation utilizing triangular elements at the macroscale.

To determine an upper bound on the error introduced by having incompatible element and RUC shapes, the effects of using 2-D, plane strain, triangular CPE3 elements on the total SERR of the model was also investigated. Figure 7 displays a typical macroscale mesh utilizing triangular elements. The dimensions of the RUC were still scaled according to Equation (**9**); however, the definition of the characteristic length of the integration point domain is no longer given by Equation (**12**). Utilizing Equation (**11**), $l_C^{I.P.}$ becomes

$$l_C^{I.P.} = \frac{\sqrt{2}}{2} l^e \tag{13}$$

for triangular elements. Additionally, the same simulations were conducted with fixed RUC dimension $L = 5.98$ μm.

4.2   Results

The total SERR of the model G was calculated using

$$G = \int \frac{\sum RF^{rightedge}}{L^{rightedge}} dU^{rightedge} - \frac{1}{2} \frac{\sum RF^{rightedge}}{L^{rightedge}} U^{rightedge} \tag{14,}$$

where $\sum RF^{rightedge}$ is the sum of the reaction forces at all the nodes on the right edge of the model, $L^{rightedge}$ is the length of the right edge (1 mm for all simulations), and $U^{rightedge}$ is the uniform displacement applied to the right edge of the model. Figure 8 displays G as a function of the characteristic length $l_C^{I.P.}$ for the various meshes. The results for the square meshes, shown in Figure 6, are indicated with square markers; whereas, the results for the triangular meshes (see Figure 7) are indicated with triangular markers. Filled markers indicate that the dimensions of microscale RUCs were scaled to satisfy Equation (9); whereas empty markers indicated that the RUC dimensions were fixed, $L = 5.98$ μm.
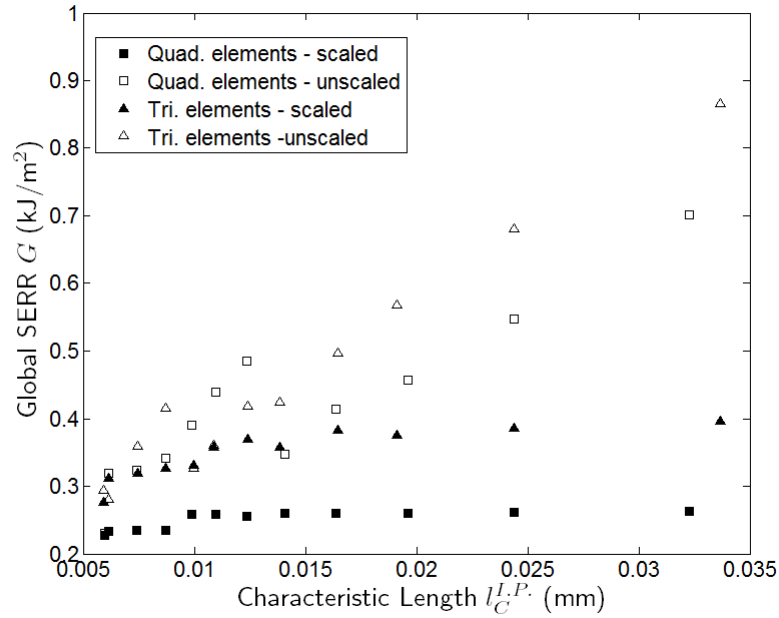

Figure 8. Total SERR of multiscale models as a function of characteristic length.

The element length that is closest to the realistic size of the RUC ($L = 5.98$ μm) is $l_C^e = 5.99$ μm (167 elements x 167 elements), and is only 0.17% larger than the actual RUC length. Thus, the scaled solution obtained with $l_C^{I.P.} = 5.99$ μm is considered to be the most accurate solution. For this mesh G was calculated to be 0.227 kJ/m^2; this value will be used as the baseline SERR for comparison with the other simulations. The most erroneous G was calculated, from the solution using the coarsest mesh $l_C^{I.P.} = 32.3$ μm, to be 0.263 kJ/m^2. Therefore, for the worst solution, G was 16% higher than the most accurate solution; although, the element length was 438.7% larger. As the mesh was refined, G approached 0.227 kJ/m^2. The maximum G, minimum G and percentage difference between the two Gs and corresponding $l_C^{I.P.}$s are presented in Table 4 for all the square and triangular mesh simulations.

Table 4. Maximum and minimum *G*, as well as corresponding $l_C^{I.P.}$, and percentage difference between Gs and $l_C^{I.P.}$.

	Quad. - scaled		Quad. - unscaled		Tri. - scaled		Tri. - unscaled	
	$l_C^{I.P.}$ (μm)	G kJ/m^2	$l_C^{I.P.}$ (μm)	G kJ/m^2	$l_C^{I.P.}$ (μm)	G kJ/m^2	$l_C^{I.P.}$ (μm)	G kJ/m^2
Max *G*	32.3	0.263	32.3	0.702	33.7	0.397	33.7	0.866
Min *G*	5.99	0.227	5.99	0.230	5.94	0.276	6.15	0.281
% Diff.	438.7	16.0	438.7	204.8	467.3	44.0	448.0	208.2

If the dimensions of the RUC were not scaled, the error observed in the SERR was very significant. The coarsest mesh exhibited $G = 0.702$ kJ/m^2 which is an error of 209.6% from the baseline. Although, when the characteristic length of the integration point domain and the size of the RUC are comparable (i.e. $l_C^{I.P.} = 5.99$ μm), $G = 0.230$ kJ/m^2, which is only difference of 1.6% from the baseline. However, the SERR calculated for the unscaled simulations dropped suddenly when the element size approached the size of the RUC. For example, the average *G* for the next three largest meshes ($l_C^{I.P.} = 6.14$ μm, 7.41 μm, and 8.70 μm) is 0.328 kJ/m^2. The SERR for the coarsest mesh is 204.8% larger than the finest mesh if the RUC dimensions are not scaled.

Clearly, scaling the size of the RUC such that it corresponds to the dimensions of the finite element minimizes the error. The variation that is observed in simulations with scaling, as the mesh is refined, can be attributed to local effects in the macroscopic FEM model such as an increase in the stress concentration ahead of the failure path front, as the mesh is refined.

The simulations incorporating triangular meshes exhibited an overall larger degree of error (when compared to the baseline) in the SERR. This is to be expected, since the shape the element and the shape of the RUC are incompatible. The characteristic length, calculated using Equation (**13**), that was closest to the assumed actual RUC length, is 5.94 μm. When the RUC dimensions were scaled, *G* was calculated to be 0.276 kJ/m^2 for this characteristic element length, an error of 21.6% from the baseline calculated using square elements. The largest *G* calculated (when RUC scaling was enforced), corresponding to the coarsest mesh with $l_C^{I.P.} = 33.7$ μm, was 0.397 kJ/m^2. The difference between the minimum *G* and maximum *G* is 44.0%, nearly three times the difference seen in simulations with square elements.

For the unscaled simulations utilizing a triangular mesh, the largest *G* calculated was 0.866 kJ/m^2, corresponding to the coarsest mesh ($l_C^{I.P.} = 33.7$ μm), and the smallest *G* calculated was 0.281 kJ/m^2, corresponding to $l_C^{I.P.} = 6.15$ μm. Note that the finest mesh ($l_C^{I.P.} = 5.94$ μm) produced an SERR of 0.294 kJ/m^2 which is slightly higher than the SERR obtained from the slightly coarser

mesh. The minimum error was 23.9%; however the difference between the maximum *G* and the minimum *G* was 208.2%. The mismatch between the element shape and the RUC shape introduces some error when compared to the baseline square solution; thus, the use of triangular elements in an FEAMAC simulation should be avoided. However, the error introduced through refining the mesh can be minimized by scaling the RUC dimension by the characteristic length of the element.

5. Conclusions

A smeared crack band model was implemented within the GMC micromechanics framework. The crack band model utilizes the characteristic length of the subcells in the micromechanics RUC to preserve the SERR of each subcell, ensuring that it is equal to the critical fracture toughness of the material and is insensitive to changes in the subcell mesh. This yields mesh objective microscale failure.

A platform for linking macroscale finite element analysis to microscale GMC computations, the FEAMAC framework developed at NASA GRC, is presented. This framework utilizes standard Abaqus and MAC/GMC input decks and data cards to setup a multiscale problem. Communication between the MAC/GMC core engine, also developed at NASA GRC, and Abaqus FEM commercial software is facilitated through an Abaqus user material UMAT subroutine.

Use of the crack band model at the microscale ensures the microscale behavior is objective with respect to changes in the GMC subcell mesh; however, it does not guarantee that the macroscopic solution will be objective with respect to the finite element mesh in a multiscale simulation. A scaling technique was developed for preserving the inherent length scale of the macroscale as the analysis proceeds into the microscale. The scaling procedure utilizes the characteristic length of the integration point domain within an element to scale the dimensions of the RUC such that the volume of the integration point domain and the RUC are equivalent. Plane strain, 2-D, uniaxial tension simulations were performed using meshes with square, triangular, and rectangular elements with, and without, scaling the RUCs for numerous degrees of mesh refinement. The overall SERR, compared to a baseline model, of each simulation is used to gauge the accuracy of the models. The technique works well when the elements are nearly square in shape, and alleviates a large degree of error observed when the scaling is not performed. Solutions using triangular elements exhibited significant error; however, the results were fairly insensitive to mesh refinement. However, changing the aspect ratio of rectangular elements significantly affected the accuracy of the solutions, and scaling the RUC by the characteristic length of the elements did not appropriately adjust the microscale problem to preserve the SERR as the mesh was changed.

6. References

1. Aboudi, J., *Mechanics of Composite Materials: A Unified Micromechanical Approach*, Elsevier, Amsterdam, Netherlands, 1991.
2. Aboudi, J., Arnold, S. M., and Bednarcyk, B. A., *Micromechanics of Composite Materials: A Generalized Approach* (in press), Elsevier, 2012.
3. Aboudi, J., Pindera, M. –J., and Arnold, S. M., "Linear Thermoelastic Higher-Order Theory for Periodic Multiphase Materials," *J. Appl. Mech.*, vol. 68, pp. 697-707, 2001.

4. Bažant, Z. P., "Can Multiscale-Multiphysics Methods Predict Softening Damage and Structural Failure?" *Mech. Amer. Acad. Mech.*, vol. 36 (5-6), pp. 5-12, 2007.

5. Bažant, Z.P., and Cedolin, L., "Blunt Crack Band Propagation in Finite Element Analysis," *J. Eng. Mech. Div.-ASCE*, vol. 105, pp. 297-315, 1979.

6. Bažant, Z.P., and Cedolin, L., *Stability of Structures: Elastic, Inelastic, Fracture and Damage Theories*, Oxford University Press, New York, NY, 1991.

7. Bažant, Z. P., and Oh, B. H., "Crack Band Theory for Fracture of Concrete," *Mater. Struct.*, vol. 16, pp. 155-177, 1983.

8. Bednarcyk, B. A., and Arnold, S. M., "MAC/GMC 4.0 User's Manual – Keywords Manual," *NASA/TM-2002-212077/VOL2*, 2002a.

9. Bednarcyk, B. A., and Arnold, S. M., "MAC/GMC 4.0 User's Manual – Example Problems Manual," *NASA/TM-2002-212077/VOL3*, 2002b.

10. Bednarcyk, B. A., and Arnold, S. M., "A Framework for Performing Multiscale Stochastic Progressive Failure Analysis of Composite Structures," *Proceedings of the 2006 Abaqus User's Conference, May 23-25, Boston, MA,* 2006.

11. Camanho, P. P., Maimí, P., and Dávila, C. G., "Prediction of Size Effects in Notched Laminates Using Continuum Damage Mechanics," *Compos. Sci. Technol.*, vol. 67, pp. 2715-2727, 2007.

12. de Borst, R., and Nauta, P., "Non-orthogonal Cracks in a Smeared Finite Element Model," *Eng. Comput.,* vol. 2, pp. 35-46, 1985.

13. deBorst, R., "Computation of Post-bifurcation and Post-failure Behavior of Strain-softening Solids," *Comput. Struct.*, vol. 25, pp. 211-224, 1987.

14. Goldberg, R. K., and Gilat, A., "Experimental and Computational Characterization of the High Strain Rate Tensile Response of Polymer Matrix Composites," *Composite Materials: Testing and Design Fourteenth Volume, ASTM STP 1436*, C. E. Bakis, Ed., ASTM International, West Conshohocken, PA, 2003.

15. Paley, M., and Aboudi, J., "Micromechanical Analysis of Composites by the Generalized Cells Model," *Mech. Mater.*, vol. 14, pp. 127-139, 1992.

16. Pietruszczak, S., and Mroz, Z., "Finite element analysis of deformation of strain softening materials," *Int. J. Numer. Methods Eng.*, vol. 17, pp. 327-334, 1981.

17. Pindera, M. –J., and Bednarcyk, B.A., "An Efficient Implementation of the GMC Micromechanics Model for Multi-phased Materials with Complex Microstructures," *NASA/CR 1997-202350*, 1997.

18. Pineda, E. J., Waas, A. M., Bednarcyk, B. A. and Arnold, S. M., "Implementation of a Smeared Crack Band Model in a Micromechanics Framework," *NASA/TM (in-press)*, 2012.

19. Pineda, E. J., Waas, A. M., Bednarcyk, B. A., Arnold, S. M., and Collier, C. S., "Multiscale Failure Analysis of Laminated Composite Panels Subjected to Blast Loading Using FEAMAC/Explicit," *NASA/TM-2009-215813*, 2009.

20. Simulia Corp., *Abaqus User's Manual, Vol. 1-3, Version 6.10-1*, Providence, RI, 2008.

21. Sullivan, R. W. and Arnold, S. M., "An Annotative Review of Multiscale Modeling and its Application to Scales Inherent in the Field of ICME," *Models, Databases, and Simulation Tools Needed for the Realization of Integrated Computational Material Engineering*, S. M. Arnold and T. T. Wong, Eds., ASTM International, Materials Park, OH, pp. 6-23, 2011.